Epigenetic remodeling via HDAC6 inhibition amplifies anti-tumoral immune responses in pediatric AML

Julian Schliehe-Diecks[†1], Jia-Wey Tu[†1], Pawel Stachura[1], Katerina Schaal[1], Marie Kemkes[1], Eleni Vasileiou[1,2], Nadine Rüchel[1], Danielle Brandes[1], Melina Vogt[1], Thomas Lenz[3], Adarsh Nair[4], Stefanie Scheu[4,5], Pilar M. Dominguez[6], Agata Pastorczak[7], Karin Nebral[8,9], Kai Stühler[3,10], Ute Fischer[1,11], Aleksandra A. Pandyra[1,2,12], Arndt Borkhardt[1,11], Sanil Bhatia[1,11*]

[1]Department of Pediatric Oncology, Hematology and Clinical Immunology, Medical Faculty, Heinrich Heine University Düsseldorf, Düsseldorf, Germany

[2]Institute of Clinical Chemistry and Clinical Pharmacology, University Hospital Bonn, 53127 Bonn, Germany

[3]Molecular Proteomics Laboratory, Biological Medical Research Center, Heinrich-Heine-University Düsseldorf, Düsseldorf, Germany

[4]Institute of Medical Microbiology and Hospital Hygiene, Heinrich Heine University Düsseldorf, Düsseldorf, Germany

[5]Institute of Immunology, Rostock University Medical Center, Rostock, Germany

[6]Université Côte d'Azur, INSERM, C3M U1065, 06204 Nice, France

[7]Department of Pediatrics, Oncology and Hematology, and Department of Genetic Predisposition to Cancer, Medical University of Lodz, Lodz, Poland

[8]St. Anna Children's Cancer Research Institute (CCRI), Vienna, Austria

[9]Labdia Labordiagnostik, Vienna, Austria

[10]Institute for Molecular Medicine, Proteome Research, University Hospital and Medical Faculty, Heinrich-Heine-University Düsseldorf, Düsseldorf, Germany

[11]German Cancer Consortium (DKTK), partner site Essen/Düsseldorf, Düsseldorf, Germany

[12]German Center for Infection Research (DZIF), Partner Site Bonn-Cologne, 53127 Bonn, German

[†] contributed equally to this work

Running Title:

HDAC6 inhibition immunomodulates AML cells

***Corresponding author**: Sanil Bhatia, Department of Pediatric Oncology, Hematology and Clinical Immunology, Heinrich Heine University Düsseldorf, Germany, Moorenstraße 5, Düsseldorf, 40225, Germany. Phone (+49) 211 81 04896; Fax; (+49) 211 81 16436 Email: sanil.bhatia@med.uni-duesseldorf.de

Competing interests

The authors declare no competing interests.

Abstract

Histone deacetylase 6 (HDAC6) has emerged as a promising therapeutic target in cancer due to its immunomodulatory effects. While its prognostic significance remains debated, we demonstrate that HDAC6 loss significantly impairs myeloid leukemia progression in vivo, despite having no functional impact on leukemia cell proliferation in vitro. Global proteome and secretome profiling of HDAC6-knockout (KO) cells revealed upregulation of several immune-related modulators, including RNase T2, a tumor suppressor known to modulate the tumor microenvironment. Notably, RNase T2 upregulation upon HDAC6 loss was restricted to myeloid but not B-ALL cells. Moreover, pharmacological inhibition of HDAC6 recapitulated this phenotype, leading to RNase T2 upregulation in myeloid leukemia cells. ATAC-seq revealed increased chromatin accessibility of RNase T2 following HDAC6 loss, highlighting a functionally epigenetic regulatory contribution. Further functional assays conducted in an immunocompetent setting both ex vivo and in vivo demonstrated that HDAC6 inhibition sensitized murine AML cells to broad $CD8^+$ T cell activation as evidenced by increased TNFα and CD107a expression. Consistently, in

a syngeneic AML model, HDAC6 inhibition restricted AML cell growth. Moreover, an extended drug screening analysis identified Cytarabine and Clofarabine as significantly synergizing with HDAC6 inhibitor (Ricolinostat) in AML cell lines or pediatric patient derived xenograft (PDX)-AML cells, while showing limited synergy in ALL cell lines, PDX-ALL cells or healthy controls. These findings suggest that HDAC6 represents a promising therapeutic target in pediatric AML by simultaneously enhancing immune activation and increasing chemosensitivity.

Graphical Abstract

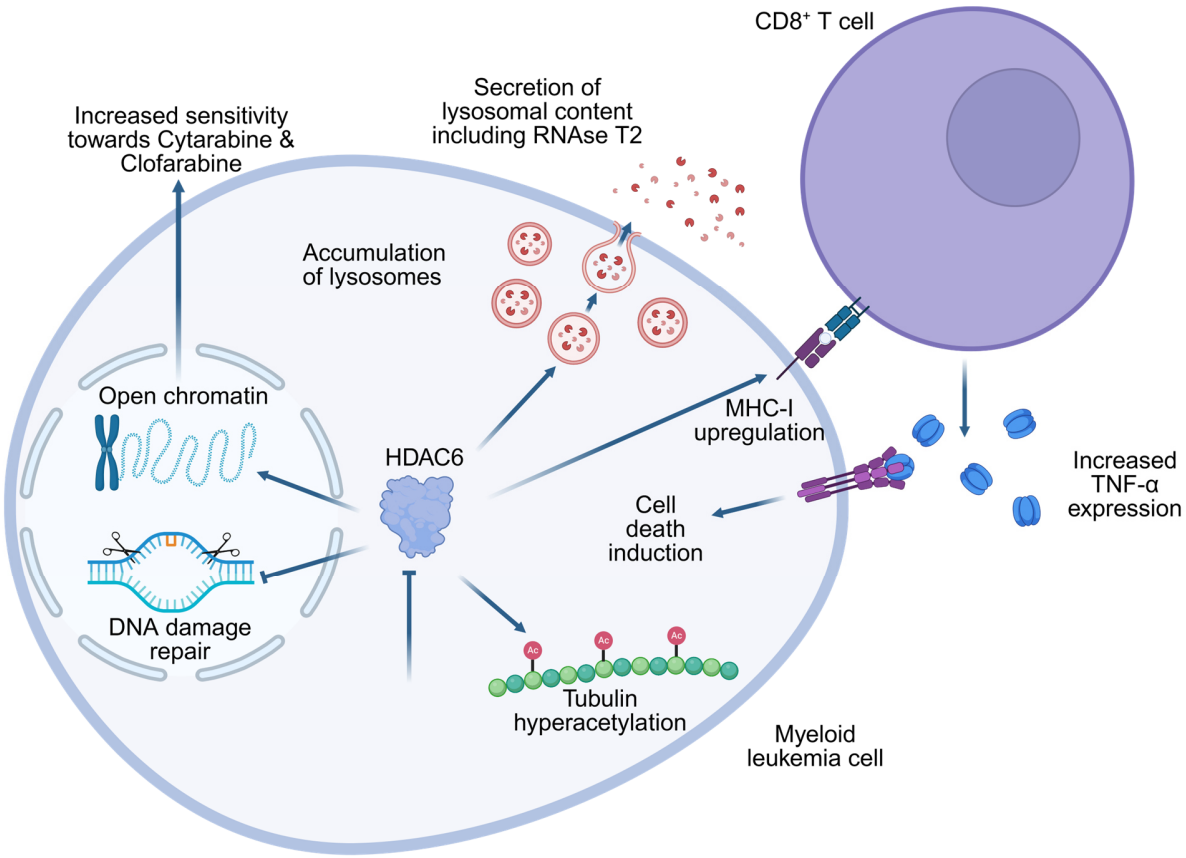

Introduction

Despite significant improvements in outcomes over the past 20 years, acute myeloid leukemia (AML) remains one of the most challenging pediatric cancers to treat.[1,2] This is compounded by the fact that the armamentarium of immunotherapeutic approaches is

narrower when compared to childhood acute lymphoblastic leukemia (ALL), where recently anti-CD19 immunotherapy revolutionized the field.[3-7] For children with AML who have clinical or genetic high-risk features as well as those with relapsed or refractory disease, stem cell transplantation remains the only definitive cure for at least a fraction of patients.[8] Thus, there is an urgent need for novel therapies. HDAC inhibitors (HDACi) have recently emerged as a promising class of therapeutics for various malignancies, including pediatric acute myeloid leukemia (pAML).[9-11] However, the approved HDACi for treating hematological malignancies are predominantly pan-HDACi, which broadly inhibit multiple HDAC isoforms involved in essential cellular functions. This lack of specificity leads to a range of adverse effects, including cardiac toxicity and severe gastrointestinal disturbances, some of which can be life-threatening.[12-14] These toxicities often require the discontinuation of HDACi-based therapies to prevent severe complications. Additionally, in clinical practice, HDACi are rarely used as monotherapy and are typically combined with other therapeutic agents, adding complexity to treatment regimens.[15,16] Selective targeting of specific HDAC isoforms may offer a promising approach to restricting their activity to particular cellular processes, potentially reducing toxicity and enhancing therapeutic tolerability.

Among the various HDAC isoforms, HDAC6 has emerged as a particularly compelling therapeutic target due to its distinct biological roles and relevance in oncogenesis.[17] HDAC6 is primarily localized in the cytoplasm and regulates a range of cellular functions through substrate deacetylation.[18-21] However, HDAC6-deficient mice remain viable and develop normally, supporting its potential as a safe therapeutic target.[22] HDAC6 is found overexpressed across various hematologic malignancies.[23-25] A recent study showed that HDAC6 inhibition suppresses leukemia stem cell expansion and reduces the proliferation of AML leukemia cell lines in a Zebrafish model.[26] These observations highlight the potential of targeting HDAC6 as a novel therapeutic approach, offering a more favorable safety profile in the treatment of hematological malignancies.[27]

Through a database-driven approach, we identified HDAC6 as a promising candidate in pAML patients as compared to childhood ALL. Using HDAC6-Knockout (KO) models and employing multi-omics characterization we identified RNase T2, a known activator of pro-

inflammatory signaling, to be upregulated upon HDAC6-KO. Further, our ex vivo and in vivo studies demonstrated that HDAC6 inhibition enhanced broad $CD8^+$ T cell activation and therefore anti-leukemic responses. Beyond its immunomodulatory role, we found that HDAC6 inhibition sensitized myeloid leukemia cells to standard chemotherapeutics. These findings highlight the potential of HDAC6 as a target in pAML, underscoring the need for further investigation into its clinical applicability.

Materials and Methods

Cell Culture: Leukemia cell lines were obtained from the DSMZ (Braunschweig, Germany) and cultured according to their recommendations. RPMI1640 GlutaMAX (Gibco) was supplemented with 10-20% fetal bovine serum and 1% penicillin/streptomycin (Sigma-Aldrich). Cell lines were regularly authenticated by short tandem repeat profiling and tested for mycoplasma.

CRISPR-Cas9 mediated knockout (KO) or shRNA-mediated knockdown (KD) of HDAC6: HDAC6-KO models were generated either through lentiviral transduction or using nucleofection of CAS9-GFP (IDT).[28] For monoclonal selection, cells were plated in semi-solid MethoCult media (Stemcell Technologies). See supplemental methods for sequences and more details.

Western blotting: Western blotting were performed as previously described.[28] For the list of antibodies and their respective concentrations, refer to the supplemental methods.

Proliferation, cell cycle and apoptosis assays: Proliferation (via Trypan Blue staining), cell cycle (via Nicoletti method) and apoptosis assay (via measuring Caspase 3/7 activity) were performed as described earlier.[28]

Colony forming unit (CFU) assay: Leukemia were seeded in a methylcellulose-based medium. After seven days, colonies (n=3) were counted and imaged, following previously described protocols.[29]

Drug screening: Ex vivo high throughput drug screening was performed as described earlier.[28,30] The compound selection comprised FDA/EMA-approved chemotherapeutics

and targeted agents commonly used in leukemia treatment protocols, along with inhibitors in various stages of clinical trials. A detailed list of drugs is provided in Supplemental Table 1. ZIP scores for the matrix synergy approach were calculated via the *Synergyfinder* R package.

qPCR: Total RNA was extracted using QIAzol and purified with the Maxwell® RSC system. cDNA was synthesized from 2 µg RNA using the QuantiTect kit, and qPCR was performed on a Bio-Rad system with B2M and GAPDH as internal controls. For more details, refer to Supplemental Methods.

Fluorescence Microscopy: Cells were seeded on poly-D-lysine–coated coverslips, fixed, permeabilized, and stained with primary/secondary antibodies and DAPI. Imaging was performed with a Zeiss Axio Observer/Apotome 3, and signal quantification was done using ImageJ. For more details, refer to Supplemental Methods.

Murine NSG transplantation: Prior to the injection K562 and MV4-11 cells were transduced with a luciferase reporter plasmid to measure the leukemic burden via the in vivo imaging system IVIS (PerkinElmer).[28] Cells were intravenously injected into 6 to 8 weeks old immunodeficient NSG mice (Jackson laboratory, #005557). For patient-derived xenograft (PDX) generation, leukemia cells from peripheral blood or bone marrow were injected into NSG mice (see Supplemental Table 2 for patient details), with engraftment monitored via FACS analysis of blood collected through orbital bleeding.[28,31] Patient material was obtained with informed consent in accordance with the Declaration of Helsinki and approved by the local ethics committees. All animal experiments were conducted in accordance with the regulatory guidelines of the official committee at LANUV (NRW), under the authorization of the animal research institute (ZETT) at the Heinrich Heine University Düsseldorf.

Murine C57BL/6J experiments: Wildtype C57BL/6J (Charles River) mice was utilized to establish murine C1498 AML (ATCC) derived syngeneic mouse model.[32] C57BL/6J wild type mice were engrafted with (0.5x10^6 cells/mouse) luciferase reporter gene transduced C1498 murine AML cell line at 6-7 weeks of age. Monitoring of the leukemic

burden and treatment with Ricolinostat followed the respective schedule. For more details, refer to Supplemental Methods.

T Cell Co-Culture Assay: C57BL/6J mice were infected with the Lymphocytic Choriomeningitis Virus (LCMV) strain, which induces a strong effector $CD8^+$ T cell response and is efficiently cleared in wild-type mice shortly after infection.[32,33] LCMV-primed splenic T cells were isolated after two weeks post infection. C1498 cells were pre-treated with Ricolinostat before co-culture with T cells. Supernatant-only and direct treatment conditions were also included. After 24 hours, cells were analyzed by flow cytometry for viability and cytokine expression. For more details, refer to Supplemental Methods.

NK Cell Killing Assay: PBMCs from healthy donors were cultured with IL-2 and IL-15. CFSE-labeled target cells were co-incubated with PBMC-derived NK cells for 4 hours, followed by flow cytometric analysis to assess NK cell-mediated cytotoxicity. For more details, refer to Supplemental Methods.

RNA-sequencing (RNA-seq), mass spectrometery (MS) based proteome and secretome anaylsis: RNA-seq and quantitative MS based proteome and secretome analysis was performed as previously described.[28] For sample preparation, cultures were maintained at a medium density for several days to harmonize viability and growth rates.

ATAC-seq: The library preparation, sequencing and initial consensus sequencing was performed according to the protocol of Active Motif. For more details, refer to Supplemental Methods.

Data mining: The HDAC6 dependency data was extracted from the Achilles gene dependency project of the DepMap (22Q1) database and visualized via complex heatmap.[34] The expression data of pediatric patients was extracted from the PeCan platform of St. Jude.[35] Expression was either clustered by leukemia subtype or separated by the median of HDAC6 expression. The survival analysis was performed using the Survival Genie 2 platform[36], utilizing data generated by the Therapeutically Applicable Research to Generate Effective Treatments (TARGET) initiative (https://www.cancer.gov/ccg/research/genome-sequencing/target), phs000218. The data

used for this analysis are available through the Genomic Data Commons (https://portal.gdc.cancer.gov). Samples were clustered by their optimal cutting point algorithm.

Data Availability: RNA-seq and ATAC-seq data have been deposited in the NCBI GEO database under accession ID: GSE297364 and GSE297366. Mass spectrometry-based proteomics and secretomics data are available via the ProteomeXchange Consortium through the PRIDE repository with dataset identifier PXD041871.

Generation of descriptive figures: The graphical Abstract and in vivo treatment schedules were created and licensed via BioRender.

Results

HDAC6 ablation impairs in vivo growth of myeloid leukemia cells

We data-mined clinical data from pediatric patients (using the *TARGET* study via survival genie 2) and found prognostic implications. High HDAC6 expression significantly correlated with poorer survival in AML, whereas in ALL, elevated HDAC6 levels were associated with improved survival outcomes (Supplemental Figure 1A-D). The analysis of over 1,500 pediatric leukemia patient samples (from the *PeCan* database) revealed a more heterogeneous HDAC6 expression pattern in AML compared to B-ALL and T-ALL (coefficient of variance or CV_{AML}=0.70 vs $CV_{B\text{-}ALL}$=0.48 or $CV_{T\text{-}ALL}$=0.39) (Supplemental Figure 1E). These findings contrast with earlier reports suggesting that selective (in vitro) HDAC6 inhibition has minimal or no cytotoxic effects on the leukemia cells.[37-39] Further, in vitro CRISPR-based dependency analysis (using data from the *DepMap* portal) also suggest that HDAC6 exhibits the lowest dependency among HDAC family members in leukemia cells (Supplemental Figure 1F).

Given these discrepancies between in vitro and in vivo HDAC6 inhibition, we employed a CRISPR-Cas9-mediated knockout (KO) approach in myeloid leukemia cells to assess the effects of HDAC6 loss. HDAC6-KO models were established in the (*BCR::ABL1*$^{+}$) K562 CML cells and (*KMT2A-r*) MV4-11 AML cells (Figure 1A-H). Loss of HDAC6 resulted in

increased α-tubulin acetylation, confirming functional impairment of HDAC6 in these models (Figure 1A and 1E). First, to evaluate the differences in the cellular growth, a proliferation assays were performed, which revealed no significant differences in doubling time between HDAC6-KO and control cells (Figure 1B and 1F). Similarly, a colony formation assay showed no alterations in clonogenic potential upon HDAC6 loss (Figure 1C and 1G). Cell cycle analysis further demonstrated minimal changes in the distribution of cells across different phases (Figure 1D and 1H). However, we observed an increased susceptibility of K562 HDAC6-KO cells to NK cell-mediated killing in an ex vivo PBMC-derived NK cell killing assay, compared to the respective controls (Supplementary Figure 1G). Notably, in an in vivo setting, HDAC6-KO (K562 and MV4-11) leukemia models exhibited a significant ($p < 0.05$) reduction in leukemia progression when transplanted into NSG mice compared to controls (Figure 1I-L). This led to a significant ($p < 0.01$) increase in overall survival in mice injected with HDAC6-KO K562 cells, while no differences in survival was observed in the MV4-11 HDAC6-KO model. (Supplemental Figure 1H-I). This discrepancy in the survival curves may be attributed to the higher aggressiveness and rapid disease kinetics of AML-derived MV4-11 cells than the CML-derived K562 cells. Taken together, our data demonstrate that despite the lack of effect on in vitro growth, HDAC6 loss inhibits progression of myeloid leukemia cells in vivo.

Targeting HDAC6 upregulates lysosomal-related protein accumulation

Building on the impaired leukemia progression observed upon HDAC6 loss, we employed quantitative mass spectrometry (MS) to profile global changes in the cellular proteome and secretome (Figure 2A-B). Gene set enrichment analysis from the proteome analysis identified multiple dysregulated functional pathways upon HDAC6 loss (Figure 2C & Supplemental Figure 2A-B). Among the most significantly ($FDR < 0.05$) enriched functional clusters in the proteomic analysis were lysosome-associated proteins, including LAMP1, LAMP2 and RNAse T2. Secretome analysis further validated an upregulation of lysosomal enzymes, suggesting increased extracellular release of lysosomal content (Figure 2B). Additionally, HDAC6-KO cells exhibited enrichment of pathways related to immune activation, inflammatory responses, MAPK signaling and cellular motility (Figure 2C). Functional enrichment analysis using STRING confirmed

significant (*FDR* < 1.E-15) changes in lysosomal and immune-related pathways, including neutrophil degranulation and innate immune system processes, among the overlapping proteins between the proteome and secretome profiles (Figure 2D and Supplemental Figure 2C-D). Using fluorescence microscopy, a significant ($p < 0.01$) increase in LAMP1 expression was validated across HDAC6-KO generated models, including K562, KCL22 and MV4-11 (Figure 2E and Supplemental Figure 2E). Next, we aimed to pharmacologically replicate the effects of HDAC6 loss using a HDAC6 inhibitor, Ricolinostat.[40,41] Ricolinostat treatment also resulted in a concentration dependent increase in the LAMP1 expression in the pediatric patient derived (*BCR::ABL1*$^{+}$) PDX-CML cells (Figure 2F). Together, these results demonstrate that targeting HDAC6 inhibition impacts lysosomal and immune-related pathways.

Targeting HDAC6 induces the expression of tumor suppressor RNase T2 in myeloid leukemia cells

Next, we selected the lysosomal lumen-associated endoribonuclease RNase T2 as a potential target downstream of HDAC6, based on its well-established role as a tumor suppressor.[42,43] Beyond its enzymatic activity, RNase T2 can trigger immune responses within the tumor microenvironment, particularly by promoting the recruitment of M1-polarized macrophages.[44,45]

Notably, all HDAC6-KO models (K562, KCL22 and MV4-11) demonstrated a consistent and significant ($p < 0.05$) upregulation of RNase T2 (Figure 3A-C). Consistent with the MS-based secretome analysis, HDAC6-KO K562 cells exhibited elevated levels of RNase T2 in the culture supernatant (Supplemental Figure 3A). Next, to determine whether this effect was specific to myeloid leukemia cells or extended to B-ALL cells, we assessed RNase T2 protein levels in HDAC6-KO or knockdown (KD) models using B-ALL cell lines (NALM6 and NALM20) and in (*BCR::ABL1*$^{+}$) PDX-ALL2 cells (Supplemental Figure 3B-E and Supplemental Table 2). Specifically, RNAse T2 expression was not upregulated upon HDAC6 loss in the tested B-ALL models. Moreover, correlation analysis (using the *PeCan* database) revealed that in AML patients, HDAC6 and RNase T2 expression levels are negatively correlated ($r = -0.13$, $p < 0.05$), whereas in lymphoid leukemia, a strong positive correlation ($r = 0.53$, $p < 0.0001$) was observed (Supplemental Figure 3F-I). These

findings suggest that high HDAC6 expression is specifically associated with reduced RNase T2 levels in AML.

Short-term treatment (24 h) with the HDAC6 inhibitor Ricolinostat (at sub-cytotoxic concentrations) also resulted in a significant ($p < 0.05$) upregulation of RNase T2 expression across multiple myeloid leukemia cell lines, including K562, THP1, and HL60 (Figure 3D-F). Additionally, we included pediatric patient derived (*BCR::ABL1*$^{+}$) PDX-CML and (*RUNX1*-mut) PDX-AML1 cells in the assay, which also revealed a concentration-dependent increase in RNase T2 levels upon treatment with Ricolinostat (Figure 3G-H and Supplemental Table 2). Immunofluorescence microscopy further confirmed that RNase T2 accumulated in a punctate pattern upon Ricolinostat treatment, in myeloid leukemia (K562, MV4-11, THP-1, and HL60) cells (Figure 3I-K and Supplemental Figure 3J). These findings suggest that HDAC6 inhibition effectively induces a phenotype characterized by a low HDAC6/RNase T2 ratio. Notably, a survival analysis (using *TARGET* dataset) showed that pAML patients with a low HDAC6/RNase T2 ratio had significantly ($p = 0.0003$) improved survival outcomes in comparison to those with a high ratio, whereas the opposite trend was observed in ALL dataset. (Supplemental Figure 3K-L). Additionally, better survival in pAML was associated with lower levels of anti-inflammatory monocytes and M2 macrophages (Supplemental Figure 3M-N), aligning with previous findings (in solid cancers) where HDAC6 inhibition or RNase T2 upregulation promotes macrophage polarization toward a pro-inflammatory phenotype.[43,46] Taken together, HDAC6 regulates RNase T2 in a lineage-specific manner.

HDAC6 inhibition enhances the accessibility at the LAMP1 and RNase T2 gene loci

Although HDAC6 primarily resides in the cytoplasm, it can localize to the nucleus and participate in chromatin regulation.[47] To investigate the mechanism underlying RNase T2 upregulation following HDAC6 loss, we performed ATAC-seq analysis. While only a limited number of genomic loci exhibited chromatin compaction following HDAC6 loss, a substantial number demonstrated increased accessibility, including loci encoding LAMP1 and RNase T2 (Figure 4A-E and Supplemental Figure 4A). Next, to assess how increased chromatin accessibility influences global gene expression, we performed RNA-seq on

HDAC6-KO cells (Supplemental Figure 4B). Gene set enrichment analysis (GSEA) on the RNA-seq data identified upregulation of pathways related to protein acetylation regulation, exocytotic vesicle secretion, and MAPK signaling, while processes associated with HDAC6 function, including aggresome and autophagosome formation, were downregulated (Supplemental Figure 4C-D).[48,49] To integrate our findings, RNA-seq data were overlaid onto the ATAC-seq dataset, revealing a substantial (24.2%) overlap between differentially accessible chromatin regions and transcriptionally upregulated genes (Supplemental Figure 4E-F). Integrated multi-omics analysis, incorporating ATAC-seq, RNA-seq, proteomic and secretomic data, revealed significant enrichment of gene sets associated with the cell periphery and plasma membrane(Figure 4F and Supplemental Figure 4G). These findings suggest that HDAC6 inhibition may regulate surface receptor expression and influence leukemia cell interactions with the surrounding microenvironment.

Pharmacological inhibition of HDAC6 using Ricolinostat or Citarinostat led to upregulation of RNase T2 transcription in AML-derived THP1 cells, as well as in PDX-CML and PDX-AML7 cells, mirroring the effects observed following genetic ablation of HDAC6 (Figure 4G and Supplemental Figure H–J). Next, to determine whether RNase T2 upregulation upon HDAC6 inhibition is reversible, we performed knock-in (KI) experiments by reintroducing HDAC6 into HDAC6-KO cells. Functional validation of HDAC6 re-expression was confirmed by the reversal of α-tubulin hyperacetylation (Figure 4I). HDAC6 restoration in HDAC6-KO cells also led to a significant ($p < 0.05$) reduction in RNase T2 expression, supporting the role of HDAC6 in the regulating RNase T2 expression.

These results demonstrate that HDAC6 inhibition induces chromatin relaxation, leading to the upregulation of RNase T2 and that this effect is reversible upon HDAC6 reintroduction.

HDAC6 inhibition sensitizes myeloid leukemia cells to CD8$^+$ T cells

Based on our multi-omics and in vivo data suggesting that targeting HDAC6 affects immune-related signaling, we aimed to further explore its immunomodulatory role in a more immunocompetent in vivo settings. We therefore utilized a syngeneic mouse model

using (C57BL/6-derived) C1498 AML cells.[50] Briefly, murine C1498-Luc-GFP+ cells were injected into immunocompetent C57BL/6 wild-type mice (Figure 5A). After confirming engraftment, the mice were treated with four doses of Ricolinostat (50 mg/kg). Bone marrow, spleen and lymph nodes were collected after the last treatment. A significant ($p < 0.05$) increase in TNFα production was observed specifically in the bone marrow (BM) infiltrating T cells harvested from Ricolinostat-treated mice, but not the spleen or lymph nodes (Figure 5B, Supplemental Figure 5A-B). Notably, BM T-cells showed an upregulation of CD107a (or LAMP1) (Figure 5C and Supplemental Figure 5C-D), a marker associated with cytotoxic T lymphocyte (CTL) lytic granule release and target cell cytotoxicity.[51]

To validate these finding, an ex vivo co-culture model was established with syngeneic murine $CD8^+$ T cells (Figure 5D). Treatment of C1498 cells with Ricolinostat induced a significant ($p < 0.01$) upregulation of GZMB, IL-2 and notably TNFα in $CD8^+$ T cells (Figure 5E). Moreover, the supernatant from Ricolinostat-treated C1498 cells was enough to elicit the same response in T cells, while Ricolinostat treatment alone did not significantly affect the expression of these markers (Figure 5F and Supplemental Figure 5E). Notably, treatment with Ricolinostat consistently enhanced $CD8^+$ T cell-mediated cytotoxicity of C1498 cells (Figure 5G). Ricolinostat treatment led to an upregulation of RNase T2 expression in murine C1498 cells, consistent with observations in human myeloid leukemia cells (Supplemental Figure 5F). Additionally, immunophenotyping of Ricolinostat-treated human K562 leukemia cells revealed a concentration-dependent increase in the HLA-ABC expression (Supplemental Figure 5G).

To further validate the involvement of HDAC6 in eliciting T cell responses, a C1498 HDAC6-KO model was generated (Supplemental Figure 5H). While the cytokine response was less pronounced with C1498 HDAC6-KO model, we still observed a significant ($p < 0.05$) increase in $CD8^+$ T cell susceptibility to cytotoxicity and cytokine responses, similar to the wild-type C1498 model upon Ricolinostat treatment (Figure 5H, Supplemental Figure 5I-J). Next, to assess the therapeutic benefit of Ricolinostat as a monotherapy, we treated wild type C57BL/6J mice following engraftment with C1498 Luc-GFP+ cells over a prolonged period (3 weeks) and monitored leukemia progression (Figure 5I). Although Ricolinostat treatment showed a trend towards restricting leukemia

progression, the results were not statistically significant, indicating that while HDAC6 inhibition enhances T cell-mediated immune responses (Figure 5J-K), and its therapeutic benefit in vivo requires additional combination partners.

Targeting HDAC6 sensitizes myeloid leukemia cells towards standard chemotherapeutics Cytarabine and Clofarabine

To further enhance the therapeutic impact of HDAC6 inhibition and identify potential anti-cancer combination partners, we conducted a synthetic lethality screen using HDAC6-KO cells (Figure 6A). HDAC6-KO cells showed significantly ($p < 0.05$) increased sensitivity to several drug classes, including tyrosine kinase inhibitors (TKIs) and anti-metabolites such as Clofarabine, Cytarabine and 5-Azacytidine. Given the clinical relevance of Cytarabine in AML, we further examined its effects alongside Clofarabine. Both drugs exhibited enhanced cytotoxicity in HDAC6-KO cells, with Clofarabine showing a particularly strong reduction in proliferation (Figure 6B, Supplemental Figure 6A). HDAC6-KO cells also displayed increased apoptosis induction ($p < 0.01$) and sub-G1 accumulation following treatment (Figure 6C-D, Supplemental Figure 6B-C). Elevated PARP cleavage ($p < 0.05$) further confirmed heightened apoptotic activity in HDAC6-KO cells compared to respective controls (Figure 6E). These findings suggest that HDAC6 loss can enhance the sensitivity to nucleoside analogs.

To validate these finding, we investigated potential synergistic interactions between Ricolinostat and Cytarabine or Clofarabine (Figure 6F-I). Both Cytarabine and Clofarabine exhibited a strong synergistic effects with Ricolinostat in K562 and MV4-11 cells. Encouraged by these findings, we extended our investigation to a broader cohort, including (n=10) AML, (n=4) B-ALL, and (n=4) T-ALL cell lines. Additionally, we included PDX-AML/CML cells derived from initial or relapsed pediatric/adult patients (n = 8), along with PDX-B-ALL (n = 5), PDX-T-ALL (n = 7), and healthy donor-derived PBMCs (n = 4), fibroblasts (n=2), mesenchymal stem cells (MSCs), cord blood-derived $CD34^+$ cells as controls (Figure 6J-M, Supplemental Figure 6D-E). Notably, myeloid lineage-derived leukemia cells from demonstrated heightened sensitivity to the HDAC6 inhibitor Ricolinostat, when combined with Clofarabine or Cytarabine, compared to B-ALL, T-ALL

and healthy control samples. Additional preclinical evaluation is warranted to assess the therapeutic potential and clinical applicability of this combination strategy.

Discussion

The primary challenge in treating pAML is chemotherapy resistance, which leads to relapse in approximately one-third of patients and results in a 5-year survival rate of <40% post relapse.[52] Recent data indicate that aberrant epigenetic modifications, including histone deacetylation, play a key role in AML leukemogenesis and may contribute to chemotherapy resistance by silencing tumor suppressor genes regulating chemosensitivity.[53]

HDAC6 has emerged as a promising anti-cancer target.[17] High HDAC6 expression correlates with poor survival in pAML patients, while in vitro (*DepMap*) and pharmacologic inhibition data show limited benefit of targeting HDAC6,[37-39] highlighting a potential disconnect between its prognostic relevance and therapeutic impact in vitro. Our in vivo findings using immunodeficient NSG mice revealed a significant reduction in leukemic progression following HDAC6 knockout, suggesting that HDAC6 loss impairs leukemogenesis, potentially via modulation of innate immune pathways that remain active in this model.[54] In line with the above, multi-omics analyses revealed activation of several immune-related pathways following HDAC6 loss, especially RNase T2, an endoribonuclease linked to pro-inflammatory macrophage activation within the tumor microenvironment.[44,45] Extending our findings to immunocompetent models, we found that HDAC6 inhibition enhanced $CD8^+$ T cell activation,[55] through TNFα induction and upregulation of CD107a (or LAMP1), aligning with emerging roles of lysosomes in T cell-mediated immunity.[56] Additionally, HDAC6 loss sensitized AML cells to nucleoside analogs Cytarabine and Clofarabine.[41] These effects were replicated with pharmacological inhibition of HDAC6 and supported by our proteomics data showing downregulation of DNA repair pathways. [57,58] Synergistic responses to HDAC6 targeting varied across tested AML cells, indicating subtype-specific sensitivity. Particularly, acute megakaryoblastic leukemia (AMKL) exhibited significantly ($p < 0.0001$) elevated HDAC6 expression compared to other AML subtypes in the PeCan dataset (Supplemental Figure

6F), warranting future studies to assess whether this correlates with increased therapeutic synergy.

Together, our study provides compelling evidence that HDAC6 inhibition enhances immune-mediated leukemia cell clearance and sensitizes myeloid leukemia cells to chemotherapeutic agents. Given the heterogeneous expression of HDAC6 across leukemia subtypes, future studies should also focus on defining biomarkers that predict response to HDAC6-targeted therapies.

Funding

This work was funded by the Deutsche Forschungsgemeinschaft (DFG, German Research Foundation) 270650915 (Research Training Group, GRK 2158). S.B. additionally acknowledges the financial support from Elterninitiative Kinderkrebsklinik e.V and DFG BH 162/4-1 (528968169).

Acknowledgements

A.B. acknowledges the financial support from Katharina-Hardt Foundation, Christiane und Claudia Hempel foundation and Löwenstern e.V.

Author Contributions

J.S-D., J.T. and S.B. performed study concept and design. J.S-D., J.T., P.S., K.S., M.K. E.V., N.R., M.V., D.B., T.L., A.N. and S.B. performed development of methodology, investigation, analysis and interpretation of data. S.S., P.D., A.S., K.N., K.S., U.F., A.A.P and A.B. contributed to resource provision, supervision, funding acquisition, and project administration. J.S-D, J.T., A.B. and S.B. performed writing, reviewing and editing of the paper. S.B. supervised this study. All authors discussed the results and commented on the manuscript.

Conflict of interest disclosures

The authors declare no competing financial interest.

References

1 Zwaan, C. M. *et al.* Collaborative Efforts Driving Progress in Pediatric Acute Myeloid Leukemia. *J Clin Oncol* **33**, 2949-2962, doi:10.1200/JCO.2015.62.8289 (2015).

2 Fornerod, M. *et al.* Integrative Genomic Analysis of Pediatric Myeloid-Related Acute Leukemias Identifies Novel Subtypes and Prognostic Indicators. *Blood Cancer Discov* **2**, 586-599, doi:10.1158/2643-3230.BCD-21-0049 (2021).

3 Hodder, A. *et al.* Blinatumomab for First-Line Treatment of Children and Young Persons With B-ALL. *J Clin Oncol* **42**, 907-914, doi:10.1200/JCO.23.01392 (2024).

4 van der Sluis, I. M. *et al.* Blinatumomab Added to Chemotherapy in Infant Lymphoblastic Leukemia. *N Engl J Med* **388**, 1572-1581, doi:10.1056/NEJMoa2214171 (2023).

5 Gupta, S. *et al.* Blinatumomab in Standard-Risk B-Cell Acute Lymphoblastic Leukemia in Children. *N Engl J Med* **392**, 875-891, doi:10.1056/NEJMoa2411680 (2025).

6 Maude, S. L. *et al.* Tisagenlecleucel in Children and Young Adults with B-Cell Lymphoblastic Leukemia. *N Engl J Med* **378**, 439-448, doi:10.1056/NEJMoa1709866 (2018).

7 Maude, S. L. *et al.* Chimeric antigen receptor T cells for sustained remissions in leukemia. *N Engl J Med* **371**, 1507-1517, doi:10.1056/NEJMoa1407222 (2014).

8 Sauer, M. G. *et al.* Hematopoietic stem cell transplantation for children with acute myeloid leukemia-results of the AML SCT-BFM 2007 trial. *Leukemia* **34**, 613-624, doi:10.1038/s41375-019-0584-8 (2020).

9 Abaza, Y. M. *et al.* Phase 1 dose escalation multicenter trial of pracinostat alone and in combination with azacitidine in patients with advanced hematologic malignancies. *Cancer* **123**, 4851-4859, doi:10.1002/cncr.30949 (2017).

10 Pommert, L. *et al.* Decitabine and vorinostat with FLAG chemotherapy in pediatric relapsed/refractory AML: Report from the therapeutic advances in childhood leukemia and lymphoma (TACL) consortium. *American journal of hematology* **97**, 613-622, doi:10.1002/ajh.26510 (2022).

11 Karol, S. E. *et al.* Safety, pharmacokinetics, and pharmacodynamics of panobinostat in children, adolescents, and young adults with relapsed acute myeloid leukemia. *Cancer* **126**, 4800-4805, doi:10.1002/cncr.33156 (2020).

12 Shah, R. R. Safety and Tolerability of Histone Deacetylase (HDAC) Inhibitors in Oncology. *Drug Saf* **42**, 235-245, doi:10.1007/s40264-018-0773-9 (2019).

13 Chen, J., Ren, J. J., Cai, J. & Wang, X. Efficacy and safety of HDACIs in the treatment of metastatic or unresectable renal cell carcinoma with a clear cell phenotype: A systematic review and meta-analysis. *Medicine (Baltimore)* **100**, e26788, doi:10.1097/MD.0000000000026788 (2021).

14 Gryder, B. E., Sodji, Q. H. & Oyelere, A. K. Targeted cancer therapy: giving histone deacetylase inhibitors all they need to succeed. *Future Med Chem* **4**, 505-524, doi:10.4155/fmc.12.3 (2012).
15 Suraweera, A., O'Byrne, K. J. & Richard, D. J. Combination Therapy With Histone Deacetylase Inhibitors (HDACi) for the Treatment of Cancer: Achieving the Full Therapeutic Potential of HDACi. *Front Oncol* **8**, 92, doi:10.3389/fonc.2018.00092 (2018).
16 Zhou, M. *et al.* Combining histone deacetylase inhibitors (HDACis) with other therapies for cancer therapy. *Eur J Med Chem* **226**, 113825, doi:10.1016/j.ejmech.2021.113825 (2021).
17 Li, T. *et al.* Histone deacetylase 6 in cancer. *J Hematol Oncol* **11**, 111, doi:10.1186/s13045-018-0654-9 (2018).
18 Hubbert, C. *et al.* HDAC6 is a microtubule-associated deacetylase. *Nature* **417**, 455-458, doi:10.1038/417455a (2002).
19 Zhang, X. *et al.* HDAC6 modulates cell motility by altering the acetylation level of cortactin. *Molecular cell* **27**, 197-213, doi:10.1016/j.molcel.2007.05.033 (2007).
20 Kovacs, J. J. *et al.* HDAC6 regulates Hsp90 acetylation and chaperone-dependent activation of glucocorticoid receptor. *Molecular cell* **18**, 601-607, doi:10.1016/j.molcel.2005.04.021 (2005).
21 Ryu, H. W. *et al.* HDAC6 deacetylates p53 at lysines 381/382 and differentially coordinates p53-induced apoptosis. *Cancer letters* **391**, 162-171, doi:10.1016/j.canlet.2017.01.033 (2017).
22 Zhang, Y. *et al.* Mice lacking histone deacetylase 6 have hyperacetylated tubulin but are viable and develop normally. *Molecular and cellular biology* **28**, 1688-1701, doi:10.1128/mcb.01154-06 (2008).
23 Maharaj, K. *et al.* Silencing of HDAC6 as a therapeutic target in chronic lymphocytic leukemia. *Blood advances* **2**, 3012-3024, doi:10.1182/bloodadvances.2018020065 (2018).
24 Losson, H., Schnekenburger, M., Dicato, M. & Diederich, M. HDAC6-an Emerging Target Against Chronic Myeloid Leukemia? *Cancers* **12**, doi:10.3390/cancers12020318 (2020).
25 Bradbury, C. A. *et al.* Histone deacetylases in acute myeloid leukaemia show a distinctive pattern of expression that changes selectively in response to deacetylase inhibitors. *Leukemia* **19**, 1751-1759, doi:10.1038/sj.leu.2403910 (2005).
26 Pezzotta, A. *et al.* HDAC6 inhibition decreases leukemic stem cell expansion driven by Hedgehog hyperactivation by restoring primary ciliogenesis. *Pharmacol Res* **183**, 106378, doi:10.1016/j.phrs.2022.106378 (2022).
27 Hackanson, B. *et al.* HDAC6 as a target for antileukemic drugs in acute myeloid leukemia. *Leuk Res* **36**, 1055-1062, doi:10.1016/j.leukres.2012.02.026 (2012).
28 Vogt, M. *et al.* Co-targeting HSP90 alpha and CDK7 overcomes resistance against HSP90 inhibitors in BCR-ABL1+ leukemia cells. *Cell death & disease* **14**, 799, doi:10.1038/s41419-023-06337-3 (2023).
29 Bhatia, S. *et al.* Targeting HSP90 dimerization via the C terminus is effective in imatinib-resistant CML and lacks the heat shock response. *Blood* **132**, 307-320, doi:10.1182/blood-2017-10-810986 (2018).

30 Flumann, R. *et al.* An Autochthonous Mouse Model of Myd88- and BCL2-Driven Diffuse Large B-cell Lymphoma Reveals Actionable Molecular Vulnerabilities. *Blood Cancer Discov* **2**, 70-91, doi:10.1158/2643-3230.BCD-19-0059 (2021).
31 Gebing, P. *et al.* A brain organoid/ALL coculture model reveals the AP-1 pathway as critically associated with CNS involvement of BCP-ALL. *Blood advances* **8**, 4997-5011, doi:10.1182/bloodadvances.2023011145 (2024).
32 Stachura, P. *et al.* Unleashing T cell anti-tumor immunity: new potential for 5-Nonloxytryptamine as an agent mediating MHC-I upregulation in tumors. *Mol Cancer* **22**, 136, doi:10.1186/s12943-023-01833-8 (2023).
33 Stachura, P., Stencel, O., Lu, Z., Borkhardt, A. & Pandyra, A. A. Arenaviruses: Old viruses present new solutions for cancer therapy. *Front Immunol* **14**, 1110522, doi:10.3389/fimmu.2023.1110522 (2023).
34 DepMap, Broad (2024). DepMap 24Q4 Public. Figshare+. Dataset. https://doi.org/10.25452/figshare.plus.27993248.v1.
35 McLeod, C. *et al.* St. Jude Cloud: A Pediatric Cancer Genomic Data-Sharing Ecosystem. *Cancer Discov* **11**, 1082-1099, doi:10.1158/2159-8290.CD-20-1230 (2021).
36 Dwivedi, B., Mumme, H., Satpathy, S., Bhasin, S. S. & Bhasin, M. Survival Genie, a web platform for survival analysis across pediatric and adult cancers. *Sci Rep* **12**, 3069, doi:10.1038/s41598-022-06841-0 (2022).
37 Reßing, N. *et al.* Multicomponent Synthesis, Binding Mode, and Structure-Activity Relationship of Selective Histone Deacetylase 6 (HDAC6) Inhibitors with Bifurcated Capping Groups. *Journal of medicinal chemistry* **63**, 10339-10351, doi:10.1021/acs.jmedchem.9b01888 (2020).
38 Reßing, N. *et al.* Development of Fluorinated Peptoid-Based Histone Deacetylase (HDAC) Inhibitors for Therapy-Resistant Acute Leukemia. *Journal of medicinal chemistry* **65**, 15457-15472, doi:10.1021/acs.jmedchem.2c01418 (2022).
39 Depetter, Y. *et al.* Selective pharmacological inhibitors of HDAC6 reveal biochemical activity but functional tolerance in cancer models. *International journal of cancer* **145**, 735-747, doi:10.1002/ijc.32169 (2019).
40 Vogl, D. T. *et al.* Ricolinostat, the First Selective Histone Deacetylase 6 Inhibitor, in Combination with Bortezomib and Dexamethasone for Relapsed or Refractory Multiple Myeloma. *Clinical cancer research : an official journal of the American Association for Cancer Research* **23**, 3307-3315, doi:10.1158/1078-0432.Ccr-16-2526 (2017).
41 Yee, A. J. *et al.* Ricolinostat plus lenalidomide, and dexamethasone in relapsed or refractory multiple myeloma: a multicentre phase 1b trial. *The Lancet. Oncology* **17**, 1569-1578, doi:10.1016/s1470-2045(16)30375-8 (2016).
42 Campomenosi, P. *et al.* The Potential Role of the T2 Ribonucleases in TME-Based Cancer Therapy. *Biomedicines* **11**, doi:10.3390/biomedicines11082160 (2023).
43 Wu, L., Xu, Y., Zhao, H. & Li, Y. RNase T2 in Inflammation and Cancer: Immunological and Biological Views. *Front Immunol* **11**, 1554, doi:10.3389/fimmu.2020.01554 (2020).
44 Acquati, F. *et al.* Loss of function of Ribonuclease T2, an ancient and phylogenetically conserved RNase, plays a crucial role in ovarian tumorigenesis. *Proc Natl Acad Sci U S A* **110**, 8140-8145, doi:10.1073/pnas.1222079110 (2013).
45 Acquati, F. *et al.* Innate Immune Response Regulation by the Human RNASET2 Tumor Suppressor Gene. *Front Immunol* **10**, 2587, doi:10.3389/fimmu.2019.02587 (2019).

46 Xu, G. *et al.* HDAC6-dependent deacetylation of TAK1 enhances sIL-6R release to promote macrophage M2 polarization in colon cancer. *Cell death & disease* **13**, 888, doi:10.1038/s41419-022-05335-1 (2022).
47 Wang, Z. *et al.* Genome-wide mapping of HATs and HDACs reveals distinct functions in active and inactive genes. *Cell* **138**, 1019-1031, doi:10.1016/j.cell.2009.06.049 (2009).
48 Kawaguchi, Y. *et al.* The deacetylase HDAC6 regulates aggresome formation and cell viability in response to misfolded protein stress. *Cell* **115**, 727-738, doi:10.1016/s0092-8674(03)00939-5 (2003).
49 Wang, R. *et al.* ATP13A2 facilitates HDAC6 recruitment to lysosome to promote autophagosome-lysosome fusion. *The Journal of cell biology* **218**, 267-284, doi:10.1083/jcb.201804165 (2019).
50 Mopin, A., Driss, V. & Brinster, C. A Detailed Protocol for Characterizing the Murine C1498 Cell Line and its Associated Leukemia Mouse Model. *Journal of visualized experiments : JoVE*, doi:10.3791/54270 (2016).
51 Betts, M. R. *et al.* Sensitive and viable identification of antigen-specific CD8+ T cells by a flow cytometric assay for degranulation. *Journal of immunological methods* **281**, 65-78, doi:10.1016/s0022-1759(03)00265-5 (2003).
52 Rasche, M. *et al.* Survival Following Relapse in Children with Acute Myeloid Leukemia: A Report from AML-BFM and COG. *Cancers* **13**, doi:10.3390/cancers13102336 (2021).
53 Huang, H. T. & Figueroa, M. E. Epigenetic deregulation in myeloid malignancies. *Blood* **138**, 613-624, doi:10.1182/blood.2019004262 (2021).
54 Hu, Z., Van Rooijen, N. & Yang, Y. G. Macrophages prevent human red blood cell reconstitution in immunodeficient mice. *Blood* **118**, 5938-5946, doi:10.1182/blood-2010-11-321414 (2011).
55 Kovalovsky, D. *et al.* The HDAC6 inhibitor AVS100 (SS208) induces a pro-inflammatory tumor microenvironment and potentiates immunotherapy. *Science advances* **10**, eadp3687, doi:10.1126/sciadv.adp3687 (2024).
56 Jin, J., Zhang, H., Weyand, C. M. & Goronzy, J. J. Lysosomes in T Cell Immunity and Aging. *Front Aging* **2**, 809539, doi:10.3389/fragi.2021.809539 (2021).
57 Namdar, M., Perez, G., Ngo, L. & Marks, P. A. Selective inhibition of histone deacetylase 6 (HDAC6) induces DNA damage and sensitizes transformed cells to anticancer agents. *Proc Natl Acad Sci U S A* **107**, 20003-20008, doi:10.1073/pnas.1013754107 (2010).
58 Jin, J. *et al.* Human HDAC6 senses valine abundancy to regulate DNA damage. *Nature* **637**, 215-223, doi:10.1038/s41586-024-08248-5 (2025).

Fig.1

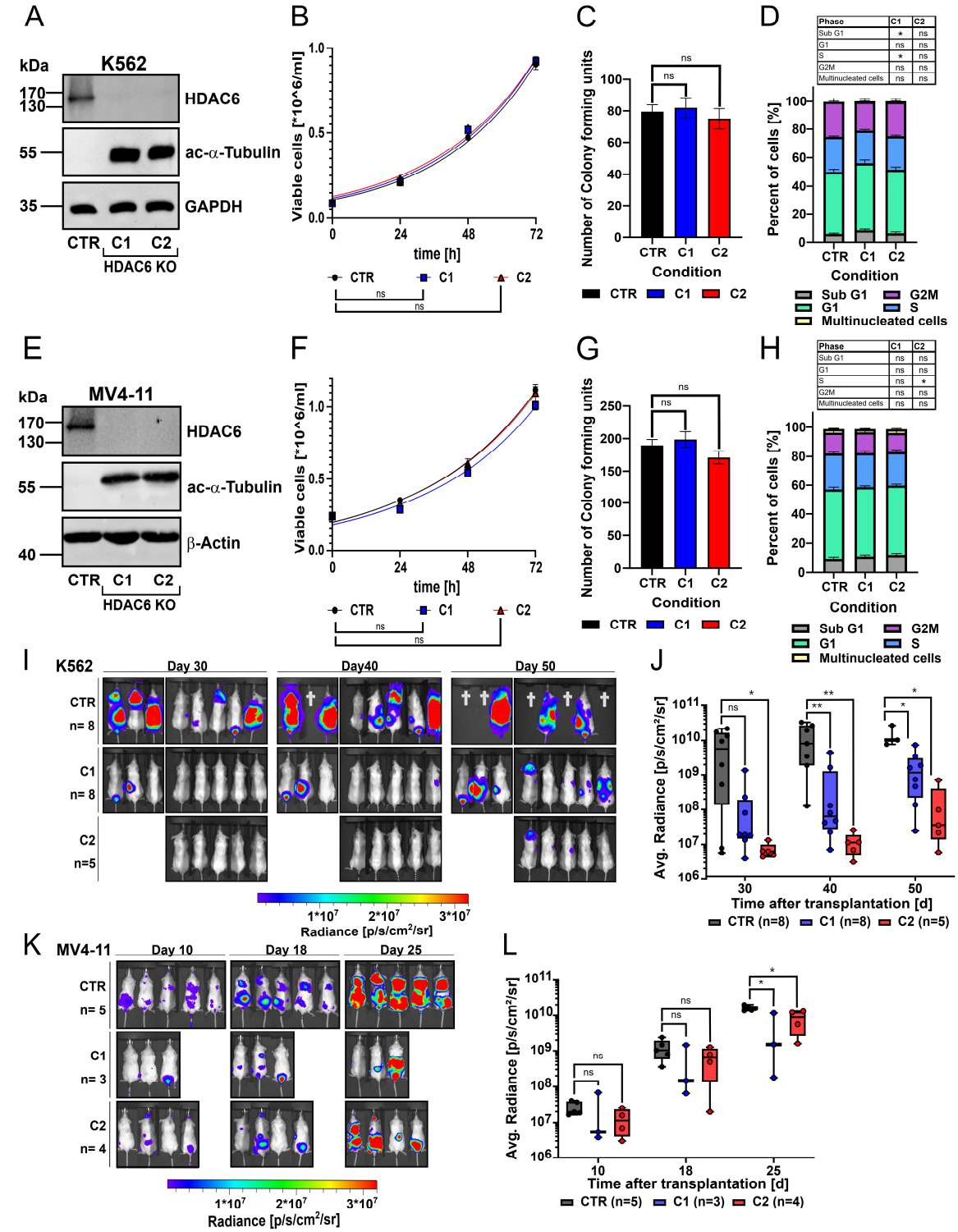

Figure 1. HDAC6 ablation impairs the in vivo growth of myeloid leukemia cells. (A) Representative western blot for HDAC6 and acetylated α-tubulin protein levels in 2 clones of K562 HDAC6-knockout (KO) (C1 & C2) and a non-targeting control (CTR) (n=3). (B) Proliferation curve determined by trypan blue assay

of K562 HDAC6-KO. Statistical significance was calculated by comparing the doubling time of the growth curve (unpaired t-test, ns = not significant, n = 3). (C) Colony forming unit (CFU) assay performed by seeding K562 HDAC6-KO cells in a semi-solid medium (unpaired t-test, ns = not significant, n = 3). (D) Bar plot showing cell cycle of K562 HDAC6-KO analysis (unpaired t-test, ns = not significant, n = 3). (E-H) Similarly, analysis were performed in the MV4-11 HDAC6-KO model, including western blot (E), proliferation assay (F), CFU assay (G) and cell cycle analysis (H) (unpaired t-test ns = not significant, *$p < 0.05$, n = 3). (I-K) *In vivo* growth kinetics of K562 (I) and MV4-11 (K) leukemia cells in NSG mice, monitored at the indicated time points post-injection using bioluminescence imaging. (J-L) Quantification of the average radiance of (I-K) for K562 (J) and MV4-11 (L) models (Mann-Whitney U-test, ns = not significant, *$p < 0.05$, **$p < 0.01$, ***$p < 0.001$).

Fig.2

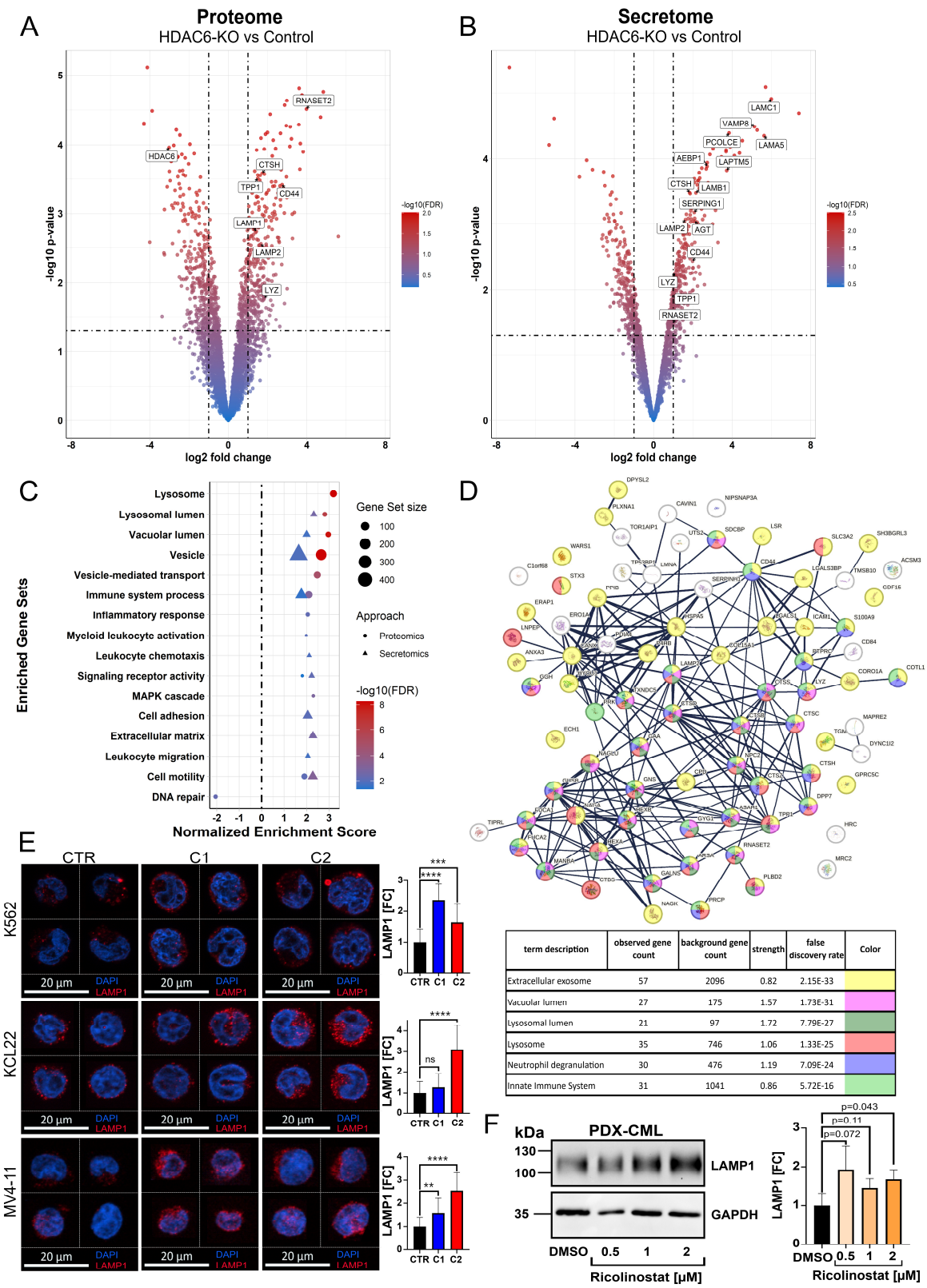

term description	observed gene count	background gene count	strength	false discovery rate	Color
Extracellular exosome	57	2096	0.82	2.15E-33	
Vacuolar lumen	27	175	1.57	1.73E-31	
Lysosomal lumen	21	97	1.72	7.79E-27	
Lysosome	35	746	1.06	1.33E-25	
Neutrophil degranulation	30	476	1.19	7.09E-24	
Innate Immune System	31	1041	0.86	5.72E-16	

Figure 2. Targeting HDAC6 upregulates lysosome-related protein accumulation. (A-B) Volcano plot depicting the cellular (A) or secreted (B) protein log2 fold change against the negative log_{10}(p-value) determined from five independent replicates of K562 HDAC6-KO (C1). Cut off for the log2 fold change was set to >1 while for the -log_{10}(p-value) >1.301 (equals <0.05) was used. The color code represents the -log_{10}(FDR) (Significance analysis of microarrays method, n= 4-5). (C) Dot plot showing the manually curated enriched gene sets obtained by a *clusterprofiler* analysis for both proteome and secretome results. The FDR cut off for inclusion of protein entries was set to < 0.1 (Kolmogorov-Smirnov test, Benjamini-Hochberg correction). (D) Protein interaction network of the overlapping proteins that were enriched both in the proteomics and secretomics analysis via string. Inclusion criteria was a shared positive direction of enrichment and a FDR < 0.1 (hypergeometric test, Benjamini-Hochberg correction). (E) Fluorescence microscopy analyzing the localization and amount of LAMP1 in K562, KCL22 and MV4-11 HDAC6-KO models. Representative cells are shown while in the right panel the bar graph compares the fold change of fluorescence signal across all analyzed cells (unpaired t-test, ns= not significant, **p < 0.01, ***p < 0.001, ****p < 0.0001, n=20). (F) Western blot analysis of LAMP1 and GAPDH expression of PDX-CML cells treated with Ricolinostat, and in the right panel quantification results normalized to GAPDH (unpaired t-test, n=3).

Fig.3

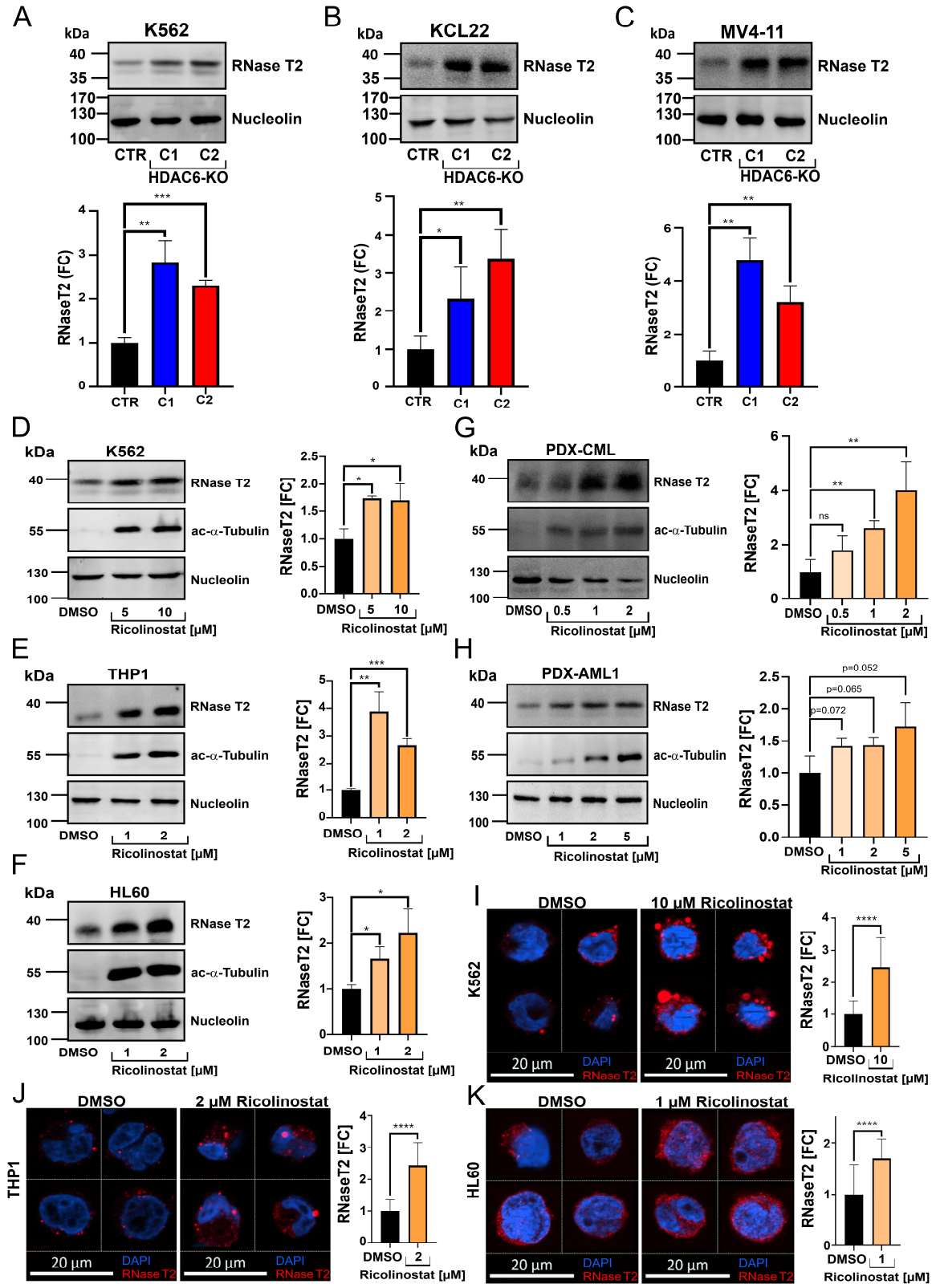
A
kDa
K562
40
35
170
130
100
RNase T2
Nucleolin
CTR C1 C2
HDAC6-KO
RNaseT2 (FC)
B
KCL22
C
MV4-11
D
ac-α-Tubulin
DMSO 5 10
Ricolinostat [μM]
RNaseT2 [FC]
E
THP1
DMSO 1 2
F
HL60
G
PDX-CML
DMSO 0.5 1 2
H
PDX-AML1
DMSO 1 2 5
p=0.052
p=0.065
p=0.072
ns
I
DMSO
10 μM Ricolinostat
K562
20 μm
DAPI
RNase T2
J
2 μM Ricolinostat
THP1
K
1 μM Ricolinostat
HL60

Figure 3. Targeting HDAC6 induces the expression of tumor suppressor RNase T2 in myeloid leukemia cells. (A-C) Western blot analysis of RNase T2 expression in HDAC6-KO myeloid leukemia models: K562 (A), KCL22 (B) and MV4-11 (C), and in the lower panel quantification results in form of a bar graph (unpaired t-test, **p<0.01, ***p<0.001, n=3). (D-H) Western blot analysis of RNase T2 and acetylated α-tubulin levels in K562 (D), THP-1 (E), HL60 (F), PDX-CML (G) and PDX-AML1 (H) cells following 24-hour treatment with the HDAC6 inhibitor Ricolinostat at the indicated concentrations. The right panel shows the results of the quantification normalized to housekeeper Nucleolin (unpaired t-test, *p<0.05, **p<0.01, ***p<0.001, n=3). (I-K) Fluorescence microscopy analysis of RNase T2 localization and expression in K562 (I), THP-1 (J), and HL60 (K) cells treated with Ricolinostat for 24 hours at the indicated concentrations. Representative cells are shown, while in the right panel the bar graph compares the fold change of fluorescence signal across all analyzed cells (unpaired t-test, ns = not significant, ****p<0.0001, n=20).

Fig.4

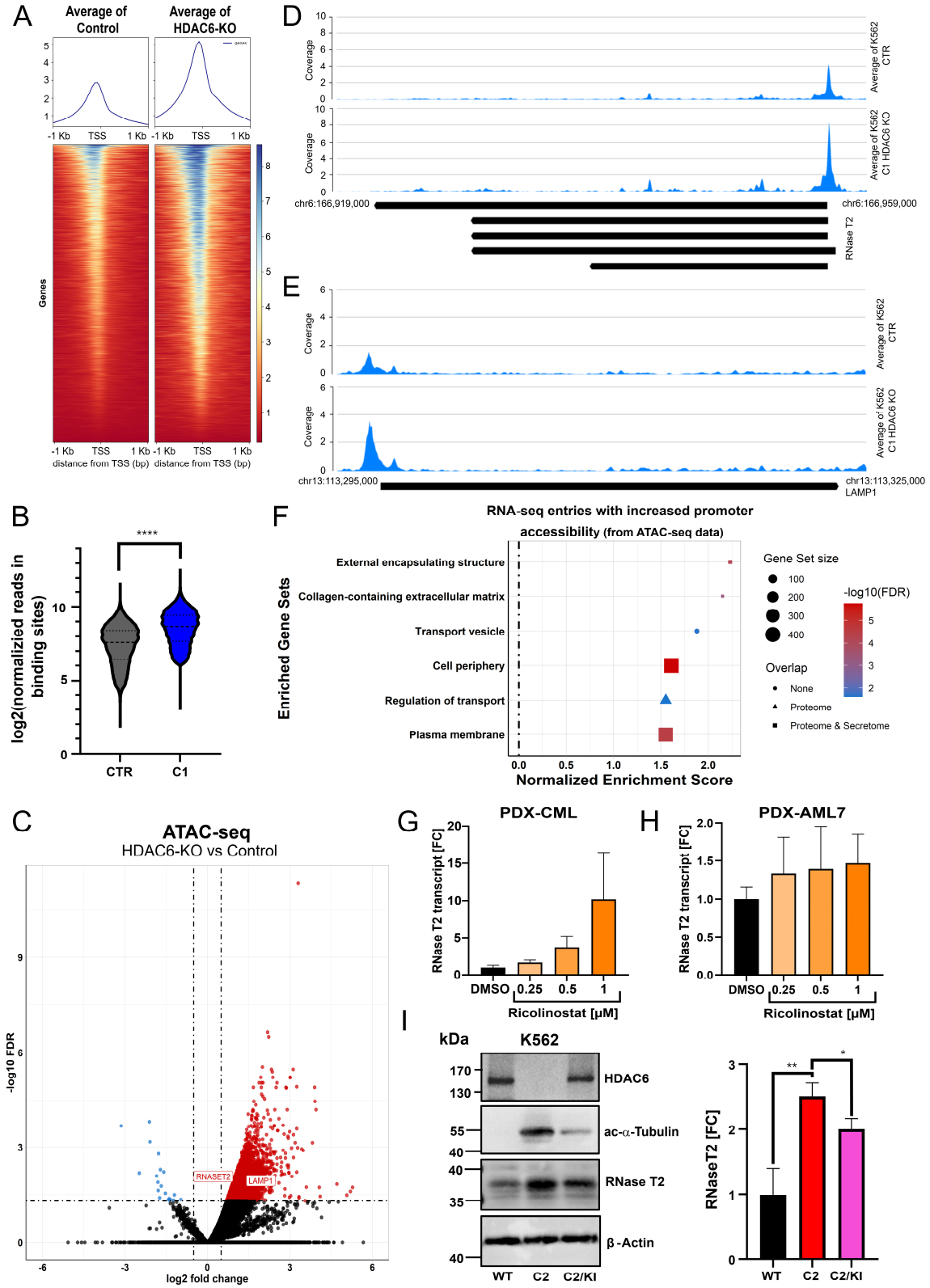
A
Average of Control
Average of HDAC6-KO
-1 Kb
TSS
1 Kb
Genes
distance from TSS (bp)
B
****
log2(normalizied reads in binding sites)
CTR
C1
C
ATAC-seq
HDAC6-KO vs Control
-log10 FDR
log2 fold change
RNASET2
LAMP1
D
Coverage
Average of K562 CTR
Average of K562 C1 HDAC6 KO
chr6:166,919,000
chr6:166,959,000
RNase T2
E
chr13:113,295,000
chr13:113,325,000
LAMP1
F
RNA-seq entries with increased promotor accessibility (from ATAC-seq data)
Enriched Gene Sets
External encapsulating structure
Collagen-containing extracellular matrix
Transport vesicle
Cell periphery
Regulation of transport
Plasma membrane
Normalized Enrichment Score
Gene Set size
-log10(FDR)
Overlap
None
Proteome
Proteome & Secretome
G
PDX-CML
RNase T2 transcript [FC]
DMSO
Ricolinostat [μM]
H
PDX-AML7
I
kDa
K562
HDAC6
ac-α-Tubulin
RNase T2
β-Actin
WT
C2
C2/KI
RNaseT2 [FC]

Figure 4. HDAC6 inhibition enhances the accessibility at the LAMP1 and RNase T2 gene loci. (A) Heatmap illustrating the distribution of chromatin accessibility relative to the transcription start site (TSS) in control (CTR) and HDAC6-KO (C1) K562 cells, as determined by ATAC-seq (n=2). (B) Violin plot comparing the log_2-normalized read density at the binding sites of all significantly enriched genes between CTR and HDAC6-KO (Mann-Whitney U-test, ****p<0.0001, n=10,577). (C) Volcano plot depicting differentially accessible chromatin regions in HDAC6-KO C1 versus CTR cells, with the log_2 fold change plotted against the $-log_{10}$(p-value). The cut-off thresholds were set at log_2 fold change > 0.5 and $-log_{10}$(FDR) > 1.301 (quasi-likelihood F-test, Benjamini-Hochberg correction, n=2). (D-E) ATAC-seq track plots illustrating chromatin accessibility at the RNase T2 (D) and LAMP1 (E) loci in CTR and HDAC6-KO K562 cells. (F) Dot plot showing the manually curated enriched gene sets obtained by a *clusterprofiler* analysis for the significant RNA-seq entries with significantly increased accessibility in the promotor region (FDR<0.05). The shape of the dot indicates whether the term was also significantly upregulated in the Proteome or Secretome (Kolmogorov-Smirnov test, Benjamini-Hochberg correction). (G-H) Quantitative PCR analysis of RNase T2 expression in PDX-CML (G), and PDX-AML7 (H) samples treated with Ricolinostat for 72 hours at the indicated concentrations. Expression levels were normalized to β-actin and B2M (n=3). (I) Western blot analysis of RNase T2 acetylated α-tubulin levels in K562 control (CTR), HDAC6-KO (C2), and HDAC6-KO (C2) with HDAC6 knock-in (C2/KI). The right panel (bar graph) shows the results of the quantification normalized to housekeeper β-actin (unpaired t-test, *p<0.05, **p<0.01, n=3).

Fig.5

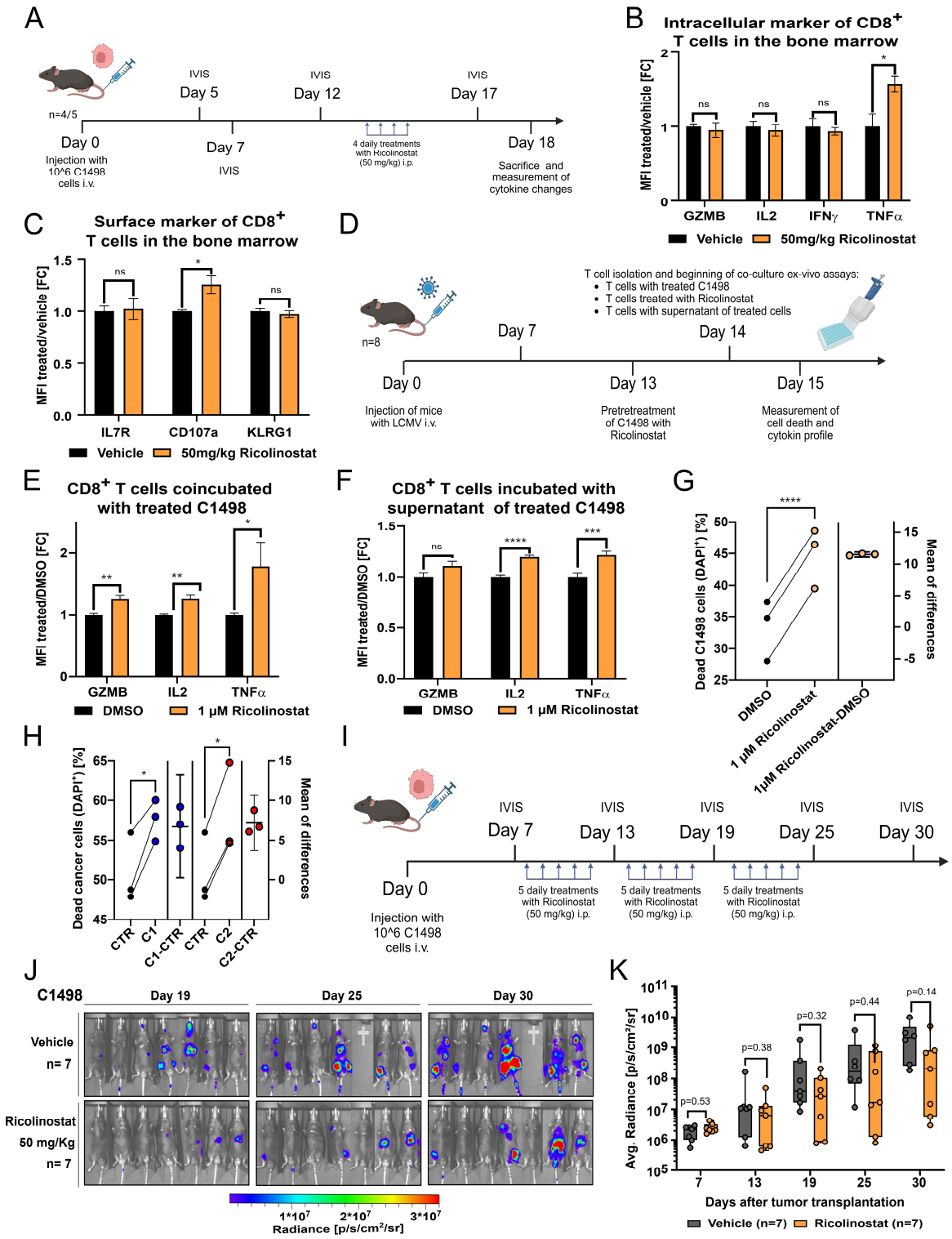
A
n=4/5
Day 0
Injection with 10^6 C1498 cells i.v.
IVIS
Day 5
Day 7
IVIS
IVIS
Day 12
IVIS
Day 17
4 daily treatments with Ricolinostat (50 mg/kg) i.p.
Day 18
Sacrifice and measurement of cytokine changes
B
Intracellular marker of CD8+ T cells in the bone marrow
MFI treated/vehicle [FC]
ns
ns
ns
*
GZMB
IL2
IFNγ
TNFα
Vehicle
50mg/kg Ricolinostat
C
Surface marker of CD8+ T cells in the bone marrow
MFI treated/vehicle [FC]
ns
*
ns
IL7R
CD107a
KLRG1
Vehicle
50mg/kg Ricolinostat
D
n=8
T cell isolation and beginning of co-culture ex-vivo assays:
• T cells with treated C1498
• T cells treated with Ricolinostat
• T cells with supernatant of treated cells
Day 0
Injection of mice with LCMV i.v.
Day 7
Day 13
Pretretreatment of C1498 with Ricolinostat
Day 14
Day 15
Measurement of cell death and cytokin profile
E
CD8+ T cells coincubated with treated C1498
MFI treated/DMSO [FC]
**
**
*
GZMB
IL2
TNFα
DMSO
1 μM Ricolinostat
F
CD8+ T cells incubated with supernatant of treated C1498
MFI treated/DMSO [FC]
ns
****
***
GZMB
IL2
TNFα
DMSO
1 μM Ricolinostat
G
Dead C1498 cells (DAPI+) [%]
Mean of differences
****
DMSO
1 μM Ricolinostat
1μM Ricolinostat-DMSO
H
Dead cancer cells (DAPI+) [%]
Mean of differences
*
*
CTR
C1
C1-CTR
CTR
C2
C2-CTR
I
Day 0
Injection with 10^6 C1498 cells i.v.
IVIS
Day 7
IVIS
Day 13
IVIS
Day 19
IVIS
Day 25
IVIS
Day 30
5 daily treatments with Ricolinostat (50 mg/kg) i.p.
5 daily treatments with Ricolinostat (50 mg/kg) i.p.
5 daily treatments with Ricolinostat (50 mg/kg) i.p.
J
C1498
Day 19
Day 25
Day 30
Vehicle
n= 7
Ricolinostat
50 mg/Kg
n= 7
1*10^7
2*10^7
3*10^7
Radiance [p/s/cm²/sr]
K
Avg. Radiance [p/s/cm²/sr]
p=0.53
p=0.38
p=0.32
p=0.44
p=0.14
7
13
19
25
30
Days after tumor transplantation
Vehicle (n=7)
Ricolinostat (n=7)

Figure 5. HDAC6 inhibition sensitizes myeloid leukemia cells to CD8+ T cells. (A) Experimental timeline of Ricolinostat (50 mg/kg) treatment following the injection of murine C1498-Luc-GFP+ AML cells into wild-type C57BL/6 mice to determine CD8+ T cell marker level. (B-C) Bar graph comparing the fold change in mean fluorescence intensity (MFI) of intracellular (B) or surface (C) marker of $CD8^+$ T cells from the bone marrow after Ricolinostat treatment against the control (unpaired t-test, ns = not significant, *$p < 0.05$, n = 4-5). (D) Experimental timeline for the harvest of primed $CD8^+$ T cells from C57BL/6 mice following Lymphocytic Choriomeningitis Virus (LCMV) injection, followed by ex vivo co-culture with C1498 cells. (E-F) Bar graph showing the fold change in MFI of quantified cytokines from $CD8^+$ T cells co-incubated with C1498 cells treated for 24 hours with 1 µM Ricolinostat (E) or the supernatant from Ricolinostat-treated C1498 cells (F) (unpaired t-test, *$p < 0.05$, **$p < 0.01$, ***$p < 0.001$, ****$p < 0.0001$, n = 16). (G) Line plot showing the fraction of dead C1498 cells when co-incubated with $CD8^+$ T cells, pretreated with Ricolinostat or DMSO (paired t-test ,****$p < 0.0001$, n = 3). (H) Similar to (G), but using C1498 HDAC6-KO (C1 or C2) cells vs non-targeting-control (CTR). (I) Experimental timeline of Ricolinostat (50 mg/kg) treatment following the injection of murine C1498-Luc-GFP+ AML cells into wild-type C57BL/6 mice to determine disease progression. (J) *In vivo* growth kinetics of C1498 cells in C57BL/6 mice treated with Ricolinostat, assessed at 19, 25, and 30 days post-injection via luminescence detection. (K) Quantification of the average radiance from (J) (Mann-Whitney U-test, n = 7).

Fig.6

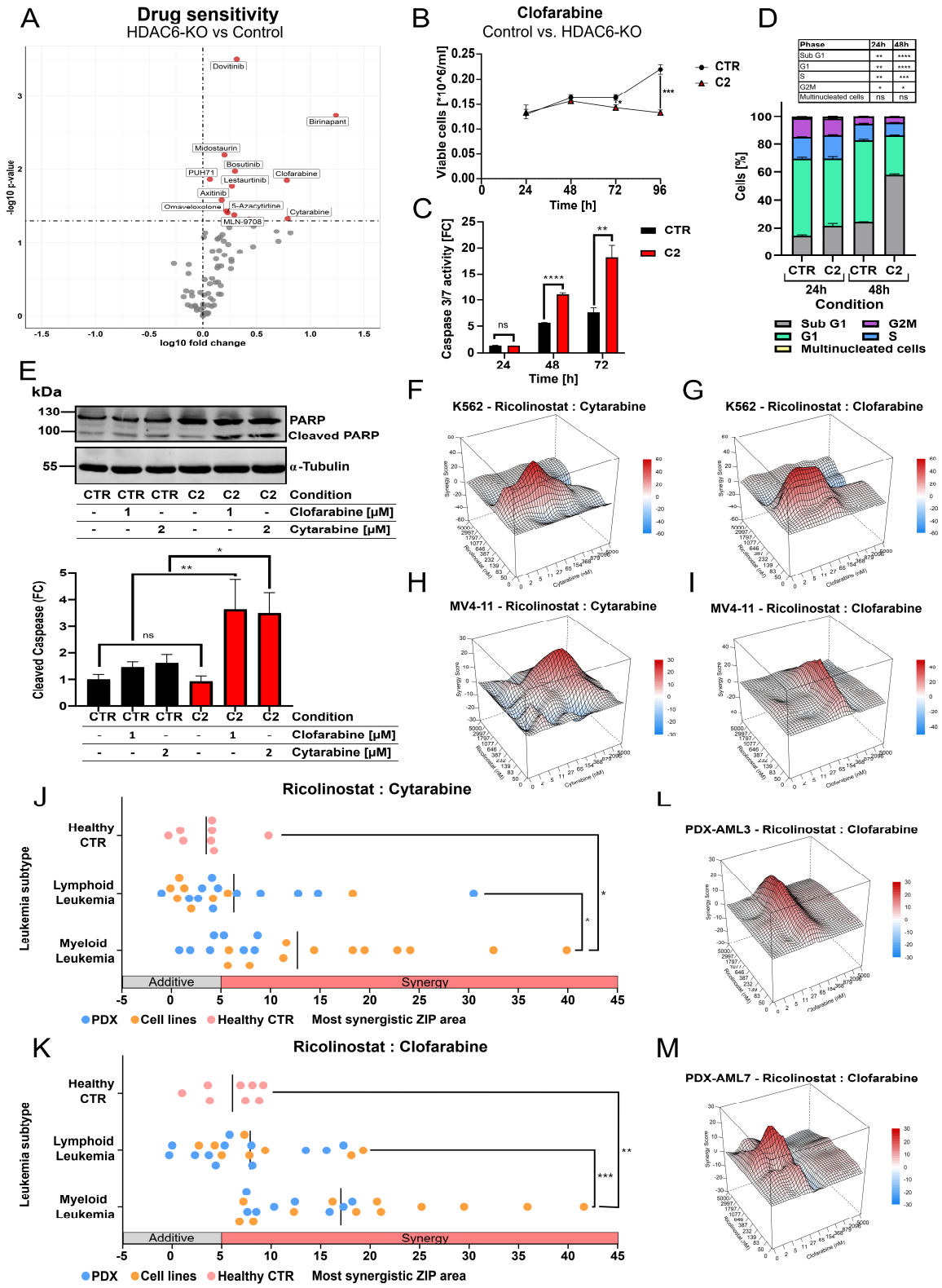
A
Drug sensitivity
HDAC6-KO vs Control
Dovitinib
Birinapant
Midostaurin
Bosutinib
PUH71
Lestaurtinib
Clofarabine
Axitinib
Omaveloxolone
5-Azacytidine
Cytarabine
MLN-9708
-log10 p-value
log10 fold change
B
Clofarabine
Control vs. HDAC6-KO
Viable cells [*10^6/ml]
Time [h]
CTR
C2
C
Caspase 3/7 activity [FC]
ns
D
Phase | 24h | 48h
Sub G1 | ** | ****
G1 | ** | ****
S | ** | ***
G2M | * | *
Multinucleated cells | ns | ns
Cells [%]
Condition
Sub G1
G1
Multinucleated cells
G2M
S
E
kDa
PARP
Cleaved PARP
α-Tubulin
Cleaved Caspase (FC)
Condition
Clofarabine [μM]
Cytarabine [μM]
F
K562 - Ricolinostat : Cytarabine
G
K562 - Ricolinostat : Clofarabine
H
MV4-11 - Ricolinostat : Cytarabine
I
MV4-11 - Ricolinostat : Clofarabine
J
Ricolinostat : Cytarabine
Leukemia subtype
Healthy CTR
Lymphoid Leukemia
Myeloid Leukemia
Additive
Synergy
PDX
Cell lines
Healthy CTR
Most synergistic ZIP area
L
PDX-AML3 - Ricolinostat : Clofarabine
K
Ricolinostat : Clofarabine
M
PDX-AML7 - Ricolinostat : Clofarabine

Figure 6. Targeting HDAC6 sensitizes myeloid leukemia cells towards standard chemotherapeutics Cytarabine and Clofarabine. (A) Volcano plot depicting the $\log_{10}$(IC50 FC) and the $-\log_{10}$(p-value) between K562 CTR and K562 HDAC6 KO (C1 and C2). As cut off was $-\log_{10}$(p-value) >1.301 (equals <0.05) used (unpaired t-test, n=3-6). (B) Proliferation curve determined by trypan blue assay of K562 CTR and K562 HDAC6-KO C2 treated with 1 µM Clofarabine over the course of 96 h (unpaired t-test, *p< 0.05, ***p< 0.001, n=3). (C) Bar plot of the fold change of the caspase 3/7 activity of K562 CTR and K562 HDAC6 KO C2 treated with 1 µM Clofarabine over the course of 72h (unpaired t-test, ns= not significant, **p < 0.05, ****p < 0.0001, n = 3). (D) Bar plot showing a cell cycle analysis of K562 HDAC6 KO models treated with Clofarabine. Statistical significance was determined via an unpaired t-test (ns= not significant, *p< 0.05, **p< 0.01, ***p< 0.001, ****p< 0.0001, n=3). (E) Western Blot analysis of PARP and cleaved PARP of K562 HDAC6 KO models treated with 1µM Clofarabine or 2 µM Cytarabine. The lower panel bar graph shows the results of the quantification of cleaved PARP normalized to the housekeeper α-tubulin (unpaired t-test, *p< 0.05, **p< 0.01, n=3). (F-I) Matrix synergy plots of K562 (F-G) and MV4-11 (H-I) depicting the combination of increasing concentrations of Ricolinostat with increasing concentrations of Cytarabine or Clofarabine. (J-K) Dot plot summarizing the most synergistic ZIP scores of AML/CML cell lines (n=12), patient-derived PDX-AML/CML cells (n=8), ALL cell lines (n=8), PDX-ALLs (n=12), and healthy controls (n=8), when treated with Ricolinostat and Cytarabine (J) or Ricolinostat and Clofarabine (K) combination. Statistical significance was determined using an unpaired t-test (ns = not significant, *p < 0.05, **p < 0.01, ***p < 0.001). (L-M) Representative matrix synergy plots of PDX-AML3 (L) and PDX-AML7 (M) cells, illustrating the synergistic effect of Ricolinostat and Clofarabine combination, as quantified in panel (K).